

Three-band superconductivity and the order parameter that breaks time-reversal symmetry

Valentin Stanev and Zlatko Tešanović

Institute for Quantum Matter and Department of Physics & Astronomy, The Johns Hopkins University, Baltimore, Maryland 21218, USA

(Received 11 January 2010; revised manuscript received 29 March 2010; published 23 April 2010)

We consider a model of multiband superconductivity, inspired by iron pnictides, in which three bands are connected via repulsive pair-scattering terms. Generically, three distinct superconducting states arise within such a model. Two of them are straightforward generalizations of the two-gap order parameter while the third one corresponds to a time-reversal symmetry-breaking order parameter, altogether absent within the two-band model. Potential observation of such a genuinely frustrated state would be a particularly vivid manifestation of the repulsive interband interactions being at the root of iron-based high-temperature superconductivity. We construct the phase diagram of this model and discuss its relevance to the iron pnictides family of high-temperature superconductors. We also study the case of the Josephson coupling between a two-band s' or $s \pm$ superconductor and a single-gap s -wave superconductor and the associated phase diagram.

DOI: [10.1103/PhysRevB.81.134522](https://doi.org/10.1103/PhysRevB.81.134522)

PACS number(s): 74.70.Xa, 74.20.Mn, 74.25.Dw

I. INTRODUCTION

The discovery of a new high-temperature superconducting (SC) family of iron-based materials¹⁻⁹ and the subsequent developments have brought the question of multiband superconductivity to the forefront of the condensed-matter research. First discussed 50 years ago, this problem had remained somewhat obscure until iron pnictides, with their multiband Fermi surfaces, made its understanding an intellectual imperative. Following the initial discovery, an order parameter (OP) based on a two-band model was proposed as a likely possibility.¹⁰ Soon thereafter, this so-called extended s -wave (or $s \pm$ or s') superconducting state has been shown to be favored by the multiband electron dynamics of iron pnictides, both within a random-phase approximation type picture¹¹⁻¹³ and in various renormalization-group-based approaches¹⁴⁻¹⁶—as well as arising from a strongly correlated local limit^{17,18}—and is currently viewed as the most plausible superconducting state for these compounds.

The first theoretical studies of a multiband superconductivity^{19,20} were a straightforward generalization of the BCS theory with gap equations for several bands and attractive interactions. The most interesting result was that the (two) superconducting gaps $\Delta^i(T)$ do not necessarily follow the single-gap BCS temperature dependence. Soon, however, it was realized²¹ that the two-band model brings something conceptually distinct—superconductivity can be enhanced even by purely repulsive interband interaction. This requires a relative minus sign between the gaps on different portions of the multiply connected Fermi surface while otherwise retaining an overall s -wave symmetry. In this way, it was argued in Ref. 21, the electron-phonon superconductivity in transition metals could receive an additional boost from the Coulomb repulsion driven resonant pair scattering between the broad s or p bands and narrow d bands at the Fermi level.

The above concept, however, extends much deeper than anticipated in Ref. 21. The purely electronic interactions could, in principle, produce superconductivity even in the *absence* of any phonon-mediated attraction. The superconductivity in this case would arise solely through the resonant

pair scattering between the two bands and both, or more as the case may be, of these bands could be narrow d or even f bands. This promising mechanism for achieving high-temperature superconductivity, using purely electron-electron interactions with cutoff on order of Fermi energy instead of Debye frequency, and thus potentially much higher transition temperature T_c —remained, however, largely ignored for the next 50 years. The reason is, basically, that the conditions in real materials are less than favorable. For s' state to be operational the superconductivity-driving interband pair scattering has to be stronger than the superconductivity-suppressing intraband repulsion (most commonly they both come from the screened Coulomb interaction in metals). This is unlikely for at least one reason: the interband interaction usually involves higher momentum transfer, bands typically being well separated in the k space, and is generically smaller. Thus, the sign-changing order parameter was considered unrealistic.

This perception changed last year with the advent of iron pnictides. At least for those members of this family that exhibit the highest T_c 's, a nodeless multigap order parameter—with some angle resolved photoemission spectroscopy (ARPES) experiments seeing as many as four different gaps²²—appears firmly established. The conventional electron-phonon interaction seems too weak to explain T_c as high as 57 K (although some highly unconventional strong electron-phonon coupling still remains a remote possibility). This state of affairs makes the purely repulsive electronic interaction as the source of superconductivity and the s' -wave state in particular very appealing, even though it is still not entirely clear how the generic repulsion problem, described in the previous paragraph, can be overcome. There are some very promising studies in this direction, based on the renormalization-group arguments and the peculiar band structure of these compounds,¹⁴⁻¹⁶ suggesting a plausible route to this superconducting state.

Many theoretical studies so far have used some variation of the two-band model. A number of useful results were derived and valuable insight was gained within this simplified picture.²³ The real materials, however, are more complex, and some tight-binding representations of iron pnictides¹⁶ indicate that typically three bands—one electron and two

holelike—are those most strongly coupled in the pair-scattering channel (see also Ref. 24). All this adds some urgency to the study of multiband superconductivity with three or four bands. In this paper, we concentrate on a rather generic three-band model with repulsive interactions. The main question we are interested in is “Is something conceptually new emerging from this increase in the number of the bands?” The answer is “Yes,” despite the fact that the gap equations themselves have the appearance of straightforward generalization of the two-band case. The reason for this is the frustration which the additional band introduces into the problem.

To develop some intuitive understanding of the model let us start with an effective two-band situation. We ignore the intraband interaction and consider only identical bands. If the coupling with the third band is negligible, there are two gaps $\Delta^1 = -\Delta^2$ and the overall magnitude is determined by the standard BCS relation. If we now introduce coupling to the additional band there are several possibilities. The system can stay in a two-gap state—now there are three such states—and keep the remaining band (nearly) gapless. In that sense, the interactions between the bands are frustrated, i.e., with such superconducting order one of the bands will not achieve what would otherwise be its natural gapped state. As suggested previously,²⁵ there is also a possibility for a different superconducting order parameter which compromises between the different frustrated two-gap order parameters. We show that this indeed happens within our microscopic model and intrinsically *complex* superconducting order parameter emerges naturally (of course, there is always an arbitrary overall phase). Such superconducting state spontaneously breaks the time-reversal symmetry and minimizes the ground-state energy for a range of coupling constants, which we determine below. For reader’s benefit, we note here that an interesting and different possible time-reversal symmetry-breaking (TRSB) order parameter, involving *s*-wave and *d*-wave coexistence, was considered in the context of pnictides in Ref. 26. Finally, if one of the Josephson-type couplings between the bands is much smaller than the other two, one intuitively expects that yet another form of the order parameter will appear: three gapped bands with a relative minus sign between the stronger-coupled ones. We show below that all of these possibilities are realized in different parts of the phase diagram of the microscopic model.

II. MODEL AND ITS GAP EQUATIONS

We start with a Hamiltonian which is a straightforward generalization of the single-band BCS theory. Our model therefore bears all the birthmarks of the original—restriction to weak coupling, omission of many details concerning band structure and dynamics of interactions, etc.—but shares some of its virtues as well: broad generality and simplicity which allows for analytic treatment. More realistic considerations would basically result in various quantitatively important but conceptually straightforward “decorations” of this simplified Hamiltonian, which we now write down in its reduced form,

$$\mathcal{H} - \mu N_{op} = \sum_{i,\mathbf{k},\sigma} \xi_{\mathbf{k}}^{(i)} c_{\mathbf{k}\sigma}^{(i)\dagger} c_{\mathbf{k}\sigma}^{(i)} + \sum_{i,j,\mathbf{k},\mathbf{k}'} G_2^{(ij)} c_{\mathbf{k}\uparrow}^{(i)\dagger} c_{-\mathbf{k}\downarrow}^{(i)\dagger} c_{\mathbf{k}'\uparrow}^{(j)} c_{-\mathbf{k}'\downarrow}^{(j)} + \text{H.c.}, \quad (1)$$

where the *i* and *j* are band indexes (they run from 1 to 3) and

for the moment we assume $G_2^{(ii)} = 0$ (i.e., *no intraband* pair scattering). This simplifies the calculations significantly and is justified by the following reasoning. If we are to include the intraband terms, there will be a finite critical strength for $G_2^{(ij)}(k, k')$, below which superconductivity cannot exist (for repulsive interactions). Above this threshold, when the superconducting state is *already present*, the intraband terms are irrelevant for the structure of the order parameter, which is entirely determined by the interband pair scattering. This argument, however, has to be applied carefully (see below). The Josephson-type term $G_2^{(ij)}(k, k')$ is separable and has the usual square-well form. We also assume identical parabolic two-dimensional bands. As we will see, in the gap equations it does not really matter whether we use hole or electron bands or some combination. So our results apply for all of these cases, although, of course, the precise dynamics that produces superconductivity in iron pnictides is most likely directly tied to its semimetallic character and the presence of both hole and electron bands at the Fermi level. This general nature of our results is the consequence of the simplified model and the relatively restricted set of question we are asking (for example, our focus is on the structure of the order parameter). We can think of Eq. (1) as describing effective low-energy theory and $G_2^{(ij)}$ as phenomenological parameters in which we have stored all the details about the realistic band structure and the high-energy processes.

Now, after we define mean-field averages

$$\Delta_{\mathbf{k}}^i = - \sum_{j \neq i, \mathbf{k}'} G_2^{(ij)}(k, k') \langle c_{-\mathbf{k}\downarrow}^j c_{\mathbf{k}\uparrow}^j \rangle \quad (2)$$

and introduce Bogoliubov-transformed fermionic operators, by using the properties of $G_2^{(ij)}$ and following the usual algebra, we get a set of three gap equations^{19,20}

$$\Delta^i = - \sum_{j \neq i} G_2^{(ij)} N^j T \sum_{\omega_n} \int_0^{\omega_c} d\xi \frac{\Delta^j}{(\omega_n)^2 + (E^j)^2}, \quad (3)$$

where $E^j = \sqrt{(\xi^j)^2 + (\Delta^j)^2}$, ω_n are the fermionic Matsubara frequencies, and ω_c is high-energy cutoff.

Despite the apparent similarity with the single-band BCS theory, these nonlinear gap equations are considerably more involved, and do not allow for analytic solutions in the general case, even at $T=0$. To achieve some progress, we need to simplify the model even further. Let us start with two bands, coupled via $G_2^{(23)}$, and then gradually turn on their couplings with a third band. We also assume these two new coupling constants $G_2^{(12)}$ and $G_2^{(13)}$ to be equal. Thus, we reduce the three generally different couplings to two and introduce dimensionless constants,

$$\lambda^{(12)} = N(0)G_2^{(12)}, \quad \lambda^{(13)} = N(0)G_2^{(13)}, \quad \lambda^{(23)} = N(0)G_2^{(23)},$$

$$\lambda^{(12)} = \lambda^{(13)} \equiv \lambda, \quad \lambda^{(23)} \equiv \eta, \quad \lambda, \eta > 0,$$

where we have denoted the density of states on the Fermi level as $N(0)$ (identical bands). With these simplifications, we are finally ready to make some analytic progress and gain some insight of the physics of our model.

III. CRITICAL TEMPERATURE AND $T \approx T_c$ REGION

We now proceed by linearizing Eq. (3) in the region $T \approx T_c$ and $|\Delta| \ll T$. The problem then reduces to finding the eigenvectors and eigenvalues of a 3×3 matrix. The possible order parameters are proportional to the eigenvectors and the eigenvalues determine T_c . In this case the Eq. (3) is equivalent to

$$I \begin{pmatrix} 0 & \lambda & \lambda \\ \lambda & 0 & \eta \\ \lambda & \eta & 0 \end{pmatrix} \begin{pmatrix} \Delta^1 \\ \Delta^2 \\ \Delta^3 \end{pmatrix} = - \begin{pmatrix} \Delta^1 \\ \Delta^2 \\ \Delta^3 \end{pmatrix} \quad (4)$$

with $I = \gamma \ln(2\omega_c / \pi T_c) > 0$ (γ is the Euler constant). Solving this matrix equation gives us three real eigenvalues

$$\delta_i = -I\eta, \quad \frac{I}{2}(\eta - \sqrt{8\lambda^2 + \eta^2}), \quad \frac{I}{2}(\eta + \sqrt{8\lambda^2 + \eta^2}), \quad (5)$$

and their corresponding eigenvectors

$$\Delta_i \propto \begin{pmatrix} 0 \\ -1 \\ 1 \end{pmatrix}, \quad \begin{pmatrix} -\frac{\eta + \sqrt{8\lambda^2 + \eta^2}}{2\lambda} \\ 1 \\ 1 \end{pmatrix}, \quad \begin{pmatrix} -\frac{\eta - \sqrt{8\lambda^2 + \eta^2}}{2\lambda} \\ 1 \\ 1 \end{pmatrix}. \quad (6)$$

For $\lambda, \eta > 0$ there are two negative eigenvalues and accordingly two possible order parameters. If we fix η and gradually increase λ from zero it is easy to see that eigenvalues δ_1 and δ_2 cross at the point $\eta = \lambda$. The $\tilde{\Delta}_1$ is obviously the two-gap solution and has higher T_c for $\lambda < \eta$. The other possibility is a three-gap superconductor with a relative minus sign between those bands that experience stronger coupling. Thus, the order parameter can be chosen to be real along the entire T_c line. Precisely at the crossing point, the eigenvalues are degenerate and there any superposition of the two eigenvectors is also a legitimate order parameter. This degeneracy is a consequence of linearizing Eq. (3) and it leads to the possibility of complex $\tilde{\Delta}$ with nontrivial phase difference between the components. One example is the $\tilde{\Delta} \propto \{1, e^{2i\pi/3}, e^{-2i\pi/3}\}$ —the Ginzburg-Landau theory of this particular state was constructed and studied in Ref. 27.

Once T is below T_c and one enters the superconducting state, we expect the complex order parameter to emerge as a competitor to the real one within a *finite* region, as opposed to a point at $T = T_c$. Because of the $2 \leftrightarrow 3$ symmetry in the gap equations, we will look for solutions that satisfy the condition $|\Delta^2| = |\Delta^3|$. We can write the ordinary two- and three-gap order parameter as

$$\tilde{\Delta}_1 = \{0, -1, 1\}\Xi, \quad \tilde{\Delta}_2 = \{-\theta, 1, 1\}\Lambda \quad (7)$$

and introduce intrinsically complex, time-reversal symmetry-breaking order parameter of the form

$$\tilde{\Delta}_3 = \{-\kappa, e^{i\varphi}, e^{-i\varphi}\}\Omega. \quad (8)$$

In Eqs. (7) and (8) $\Xi, \theta, \Lambda, \kappa, \Omega$, and φ are all real variables that parameterize the order parameters on the different bands

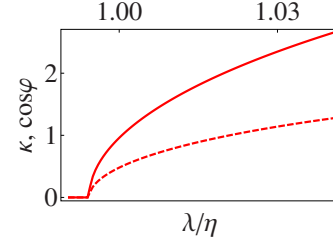


FIG. 1. (Color online) Plot of κ (solid line) and $\cos \varphi$ (dashed line) for $\tilde{\Delta}_3$ at $T = 0.95T_c$. This OP exists as a distinct solution only at a vicinity of the degenerate point $\lambda = \eta$. On the left it merges with $\tilde{\Delta}_1$ and on the right crosses $\tilde{\Delta}_2$ at $\cos \varphi = 1$ and disappears. The interval is asymmetric with respect to the degenerate point.

and are to be determined self-consistently by solving the gap equations.

To proceed analytically we expand the Eq. (3) for $(T_c - T)/T_c$ to second order in the magnitude of the order parameter. The two-gap solution obviously follows the BCS behavior,

$$\frac{1}{\eta} = \gamma \ln\left(\frac{2\omega_c}{\pi T}\right) - \beta_0 \frac{\Xi^2}{T_c^2}, \quad (9)$$

where we have simplified the notation by introducing a new constant $\beta_0 = 7\zeta(3)/8\pi^2$. The three-gap order parameters have more complicated behavior,

$$\lambda \theta(1 - \theta^2) \ln\left(\frac{2\omega_c}{\pi T}\right) + \frac{\theta^4}{2} - \frac{\eta\theta}{2\lambda} - 1 = 0, \quad (10)$$

$$\frac{\theta}{2\lambda} = \gamma \ln\left(\frac{2\omega_c}{\pi T}\right) - \beta_0 \frac{\Lambda^2}{T_c^2}$$

and

$$\lambda \kappa(1 - \kappa^2) \ln\left(\frac{2\omega_c}{\pi T}\right) + \frac{\lambda \kappa^3}{\eta} - \frac{\eta \kappa}{\lambda} = 0, \quad (11)$$

$$\cos \varphi = \frac{\eta \kappa}{2\lambda}, \quad \frac{1}{\eta} = \gamma \ln\left(\frac{2\omega_c}{\pi T}\right) - \beta_0 \frac{\Omega^2}{T_c^2}.$$

We now solve these equations numerically and obtain $\tilde{\Delta}_1, \tilde{\Delta}_2$, and $\tilde{\Delta}_3$. The TRSB solution exist only in the narrow interval $\lambda \in (\lambda_{c1}, \lambda_{c2})$, where $\lambda_{c1}, \lambda_{c2} \rightarrow \eta$ for $T \rightarrow T_c$. For λ smaller than λ_{c1} , the complex order parameter reduces to the two-gap one, while for the coupling parameter bigger than λ_{c2} only the trivial solution exist for $\tilde{\Delta}_3$ (see Fig. 1).

Using Eqs. (9)–(11) we can proceed to calculate all the thermodynamic quantities of interest. We follow a simple route—solve Eq. (10) for $\theta(T, T_c)$ and Eq. (11) for $\kappa(T, T_c)$, $\varphi(T, T_c)$ (their structure allows it). After that we construct three single-variable Ginzburg-Landau theories (assuming uniform solutions), minimize the free energies and compare the results,

$$\mathcal{F} = \alpha_i |\psi_i|^2 + \frac{\beta_i}{2} |\psi_i|^4, \quad \mathcal{F}_{min} = -\frac{\alpha_i^2}{2\beta_i}, \quad (12)$$

where $|\psi_1| = \Xi$, $|\psi_2| = \Lambda$ and $|\psi_3| = \Omega$. To do that we write the interaction part of the Hamiltonian as

$$\mathcal{H}_{int} = \sum_{i,j,k,k'} G_2^{(ij)} c_{\mathbf{k}\uparrow}^{(i)\dagger} c_{-\mathbf{k}\downarrow}^{(j)\dagger} d^j + \text{H.c.} \quad (13)$$

and in Eq. (13) we have introduced auxiliary mean-field averages $d^i = -\sum_{\mathbf{k}} \langle c_{-\mathbf{k}\downarrow}^i c_{\mathbf{k}\uparrow}^i \rangle$. Using the definitions of $\{\Delta^i\}$ we can write equations for d^i ,

$$\Delta^1 = \frac{\lambda}{N(0)} (d^1 + d^2), \quad \Delta^2 = \frac{1}{N(0)} (\lambda d^1 + \eta d^3),$$

$$\Delta^3 = \frac{1}{N(0)} (\lambda d^1 + \eta d^2),$$

which can be solved for $\{d^i\}$,

$$d^1 = N(0) \frac{-\eta \Delta^1 + \lambda (\Delta^2 + \Delta^3)}{2\lambda^2},$$

$$d^2 = N(0) \frac{\eta \Delta^1 + \lambda (-\Delta^2 + \Delta^3)}{2\lambda \eta},$$

$$d^3 = N(0) \frac{-\eta \Delta^1 + \lambda (\Delta^2 - \Delta^3)}{2\lambda \eta}.$$

Now we can obtain connected-diagrams expansion for the free energy in orders of d^i . The second- and the fourth-order terms come from the expressions

$$\mathcal{F}_2 \propto \int_0^{1/T} d\tau_1 \int_0^{1/T} d\tau_2 \langle T_\tau \mathcal{H}_{int}(\tau_1) \mathcal{H}_{int}(\tau_2) \rangle,$$

$$\mathcal{F}_4 \propto \int_0^{1/T} d\tau_1 \dots \int_0^{1/T} d\tau_4 \langle T_\tau \mathcal{H}_{int}(\tau_1) \dots \mathcal{H}_{int}(\tau_4) \rangle.$$

Using Eq. (13) for \mathcal{H}_{int} , properties of the electron Greens' functions $\mathcal{G}^{ij} \sim \delta_{ij}$ and expressing the d^i 's via the Δ^i 's we eventually get \mathcal{F} in the form of Eq. (12). We have to calculate the prefactors so we can compare the different order parameters. Expressions for $\alpha_1(T, T_c)$, $\alpha_2(T, T_c, \theta)$, $\alpha_3(T, T_c, \kappa, \varphi)$, $\beta_1(T, T_c)$, $\beta_2(T, T_c, \theta)$, and $\beta_3(T, T_c, \kappa, \varphi)$ are straightforward but tedious to obtain and very unwieldy, so we just report the results for \mathcal{F} . Far from the symmetric point $\lambda = \eta$ the solution with highest T_c remains stable. In Fig. 2 we show the comparison between different \mathcal{F} 's for $T = 0.95T_c$ at the vicinity of the symmetric point—the different solutions which are degenerate at T_c split, and the complex order parameter has lowest free energy. This, however, remains true only in a relatively small interval around the line $\lambda = \eta$, which as $T \rightarrow T_c$ reduces to a point. This interval is asymmetric and considerably smaller on the $\lambda < \eta$ side. The different phases appear to be divided by a continuous phase transition on the left and a first-order phase transition on the right side.

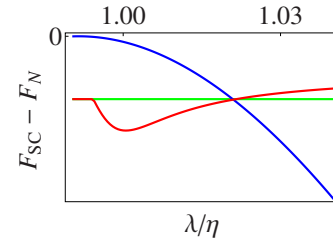


FIG. 2. (Color online) Comparison between the $\mathcal{F}_{SC} - \mathcal{F}_N$ for $\tilde{\Delta}_1$ (green), $\tilde{\Delta}_2$ (blue), and $\tilde{\Delta}_3$ (red). We show calculation on the right side of the $\lambda = \eta$ point for $T = 0.95T_c$. The free energy of the real two-gap solution is constant and of the real three-gap one decreases monotonically. The complex OP minimizes the free energy in a small interval. The transition between $\tilde{\Delta}_3$ and $\tilde{\Delta}_2$ is discontinuous.

IV. LOW-TEMPERATURE REGION

Now we will concentrate on $T = 0$ properties of the model. To distinguish the parameters from the finite-temperature case we use subscript “0.” To find Ξ_0 , θ_0 , Λ_0 , κ_0 , and Ω_0 we have to solve $T = 0$ version of Eq. (3).

The two-gap solution leads to identical gap magnitudes which obey the BCS relation,

$$\Xi_0 \approx 2\omega_c e^{-1/\eta}. \quad (14)$$

Since λ does not enter the gap equation for $\tilde{\Delta}_1$, it is always a solution, irrespective of the ratio η/λ .

For the real three-gap solution $\tilde{\Delta}_2$ there are two unknowns to determine. We get the following equations for them,

$$\theta_0^2 - \frac{\eta}{\lambda} \theta_0 - 2\theta_0 \ln \theta_0 - 2 = 0,$$

$$\Lambda_0 = 2\omega_c e^{-\theta_0/2\lambda}. \quad (15)$$

This set of equations can be solved numerically and there is always a nonzero solution for θ_0 . That means that $\tilde{\Delta}_2$ is solution for all (nonzero) values of λ . Looking at Λ_0 , however, we see that it is strongly suppressed for $\lambda \rightarrow 0$, which is to be expected since at $\lambda = 0$ the only nontrivial solution is $\tilde{\Delta}_1$.

For the complex three-gap order parameter we get equations

$$\lambda \kappa_0 \ln(\kappa_0) - \kappa_0 \left(\frac{\lambda^2 - \eta^2}{\lambda \eta} \right) = 0,$$

$$\cos \varphi_0 = \frac{\eta \kappa_0}{2\lambda}, \quad \Omega_0 = 2\omega_c e^{-1/\eta}. \quad (16)$$

These equations have nontrivial solutions for $\lambda \in (0, \lambda_{c0})$, where $\lambda_{c0} > \eta$ (see Fig. 3). At the point $\lambda = \eta$ the order parameter has the completely symmetric form

$$\tilde{\Delta}_3^{symm} = \{1, e^{2i\pi/3}, e^{-2i\pi/3}\} \Omega_0, \quad (17)$$

which is easy to understand if we consider the gap equations. At this point $\Xi_0 = \Omega_0$.

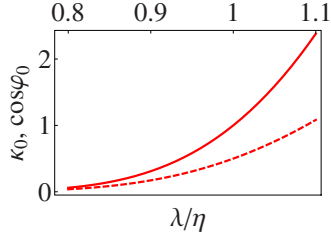


FIG. 3. (Color online) Plot of κ_0 (solid line) and $\cos \varphi_0$ (dashed line) for $\tilde{\Delta}_3$ at $T=0$. This OP exists only for $\lambda \in (0, \lambda_{c0})$, where $\lambda_{c0} > \eta$.

Now we want to see which order parameter is the actual ground state for different λ . We calculate the difference between the superconducting and the normal-state energies for the different $\tilde{\Delta}$,

$$\mathcal{E}_{SC} - \mathcal{E}_N = \langle \Psi_{\tilde{\Delta}} | \mathcal{H} - \mu N_p | \Psi_{\tilde{\Delta}} \rangle - \langle \Psi_{FS} | \mathcal{H} - \mu N_p | \Psi_{FS} \rangle.$$

The normal and superconducting state kinetic energies are, respectively,

$$\begin{aligned} \mathcal{K}\mathcal{E}_N &= \sum_{i, k < k_F} 2\xi_{\mathbf{k}}^i, \\ \mathcal{K}\mathcal{E}_{\tilde{\Delta}} &= \sum_{i, \mathbf{k}} \left[\xi_{\mathbf{k}}^i - \frac{(\xi_{\mathbf{k}}^i)^2}{E^i} \right]. \end{aligned} \quad (18)$$

Converting the sum into an integral gives

$$\begin{aligned} \mathcal{K}\mathcal{E}_{\tilde{\Delta}} - \mathcal{K}\mathcal{E}_N &= 2 \sum_i N(0) \int_0^{\omega_C} \left[\xi_{\mathbf{k}}^i - \frac{(\xi_{\mathbf{k}}^i)^2}{E^i} \right] \\ &\approx N(0) \sum_i \left[|\tilde{\Delta}^i|^2 \sinh^{-1} \left(\frac{\omega_C}{|\tilde{\Delta}^i|} \right) - \frac{1}{2} |\tilde{\Delta}^i|^2 \right]. \end{aligned} \quad (19)$$

The mean-field average of the potential energy in the normal state is zero and for calculation in the superconducting state we again use d^i . Then the potential energy can be written as

$$\mathcal{P}\mathcal{E}_{\tilde{\Delta}_i} - \mathcal{P}\mathcal{E}_N = \lambda d^{1*} d^2 + \lambda d^{1*} d^3 + \eta d^{2*} d^3 + \text{H.c.} \quad (20)$$

Using the expressions for d^i in the potential-energy formula we get

$$\begin{aligned} \mathcal{P}\mathcal{E}_{\tilde{\Delta}} - \mathcal{P}\mathcal{E}_N &= N(0) \frac{-\eta |\Delta^1|^2 + \lambda^2 (-|\Delta^2|^2 + |\Delta^3|^2)}{\lambda^2 \eta} \\ &+ N(0) \frac{\lambda \eta [\Delta^1 (\Delta^{2*} + \Delta^{3*}) + \Delta^{1*} (\Delta^2 + \Delta^3)]}{\lambda^2 \eta}. \end{aligned}$$

Combining Eqs. (19) and (20) we can compute the energies for the different possible ground states and compare them. Let us start with $\tilde{\Delta}_1$ —since Ξ_0 follows the BCS behavior we get the standard result, multiplied by 2 (two bands),

$$\mathcal{E}_{\tilde{\Delta}_1} - \mathcal{E}_N = -N(0) \Xi_0^2. \quad (21)$$

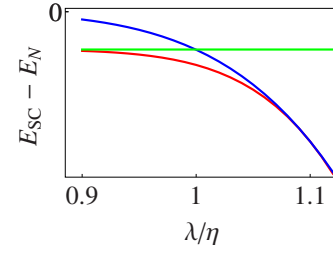


FIG. 4. (Color online) Comparison between the $\mathcal{E}_{SC} - \mathcal{E}_N$ for $\tilde{\Delta}_1$ (green), $\tilde{\Delta}_2$ (blue), and $\tilde{\Delta}_3$ (red). The first one is never a ground state for $\lambda \neq 0$. The energies for $\tilde{\Delta}_2$ and $\tilde{\Delta}_3$ merge for some $\lambda_{cr} > \eta$.

Similar calculations for $\tilde{\Delta}_2$ and $\tilde{\Delta}_3$ give the energy difference as a function of θ_0 and Λ_0 , or κ_0 and Ω_0 ,

$$\mathcal{E}_{\tilde{\Delta}_2} - \mathcal{E}_N = -N(0) \left(1 + \frac{\theta_0^2}{2} \right) \Lambda_0^2, \quad (22)$$

$$\begin{aligned} \mathcal{E}_{\tilde{\Delta}_3} - \mathcal{E}_N &= -N(0) \left[1 - \frac{2}{\eta} + \frac{\kappa_0}{2} \left(1 - \frac{2}{\eta} + 2 \ln \kappa_0 \right) \right] \Omega_0^2 - N(0) \\ &\times \left(\frac{\eta \kappa_0^2 + 4\lambda \kappa_0 \cos \varphi_0}{2\lambda^2} + \frac{2 \sin^2 \varphi_0}{\eta} \right) \Omega_0^2. \end{aligned} \quad (23)$$

Now we are able to compare the different solutions—the result is shown on Fig. 4. On the left side of η we see that the time-reversal symmetry-breaking order parameter is the ground state. It converges from below to the two-gap solution as $\lambda, \theta_0 \rightarrow 0$. At the symmetric point $\lambda = \eta$ we can use the BCS result for both solutions and $\mathcal{E}_{\tilde{\Delta}_3} - \mathcal{E}_N = 3/2 (\mathcal{E}_{\tilde{\Delta}_1} - \mathcal{E}_N)$ (three vs two gaps). On the right side there is a quantum phase transition at some $\lambda_{cr} > \eta$, where the complex and the real three-gap states merge ($\cos \varphi = 1$). Beyond this point $\tilde{\Delta}_3$ ceases to exist.

V. PHASE DIAGRAM

On the basis of the above results we suggest that our model has the phase diagram depicted in Fig. 5. There are three superconducting order parameters, stable in different regions, separated by two critical lines. On the left, different

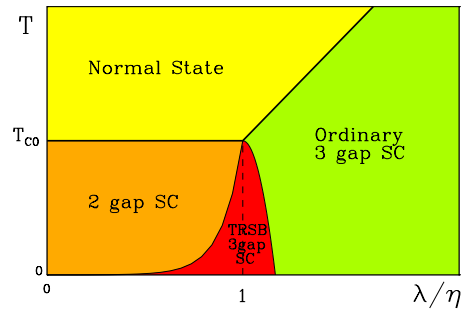


FIG. 5. (Color online) Suggested phase diagram of the three-band model. There are three possible SC OPs. The line separating the TRSB and real three-gap OP is most likely first-order phase transition line.

superconducting states appear to be separated by continuous transition and on the right by first order one at finite temperature, and continuous one at $T=0$. There is a possibility of observing two different superconducting states in a single system and the transition between them, tuned by the temperature. In the context of this phase diagram we consider the case of iron pnictides—bands 2 and 3 can be thought as the hole bands at the Γ point, which are strongly coupled to one of the electron bands at the $M=(\pi, \pi)$ point.¹⁶ If the renormalization-group arguments apply, $G_2^{e1h_i}$ are enhanced and $G_2^{h1h_2}$ is suppressed by the same high-energy electron-hole processes. Then the appropriate regime for the pnictides is $\lambda > \eta$, on the right side of our diagram. The existence of time-reversal symmetry-breaking order parameter is not excluded, but is unlikely for the optimally doped compounds, given the relative narrowness in which it is stable for $\lambda > \eta$. However it may be present in the overdoped materials, for which the interband interactions are suppressed, due to the significant deviations from perfect nesting. This complex order parameter, in general, entails the existence of local magnetic fields at edges and around impurities, and likely domain structure.²⁸ These effects may provide the best way of observing such state and its broken symmetry.

Before we proceed, let us comment on two obvious deficiencies in our model, which seemingly prevent us from applying the results we have derived thus far to the iron pnictides. First, we have completely neglected the intraband pairing terms. Once these terms are included the calculations become considerably more involved and it is difficult to proceed short of pure numerics. However, we believe that our phase diagram is qualitatively correct even in that case, since, as already explained, these terms do not play a role in determining the structure of the order parameter (provided that the superconductivity is still possible) and only change the numerical values of various results (T_c , for example). The validity of this argument is limited, however, and the intraband terms have an important role to play in the case of several competing channels (s and d waves, for example) which are affected differently by these terms. There are several studies for pnictides suggesting such competition.^{11,29,30} But as long as the most isotropic superconductivity remains the leading instability, it will be realized without any mixing from the subleading channels (for s and d mixing see Ref. 31) and our results apply. In case the system is driven to a nodal state by the intraband repulsion, the frustration due to the interband terms can again lead to a development of complex order parameter, but we leave this question for further studies. Second, we have restricted ourselves to a three-band model, whereas in pnictides there are generally four active bands participating in the superconductivity (see, for example, Ref. 22). It is a valid question if adding another band will completely suppress the complex order parameter. To address it let us remind the reader the tight-binding calculation,¹⁶ which indicates that, for the case of pnictides, the pair-scattering terms between the second electron band (whose existence we have neglected) and the hole bands are at least an order of magnitude smaller than G^{e1h_i} (analogous to our G_2^{13} and G_2^{23} terms). Coupling between the electron bands, however, generically will be of the same order as G^{h1h_2} (our G_2^{12}). This means, in practice, that the phase of the

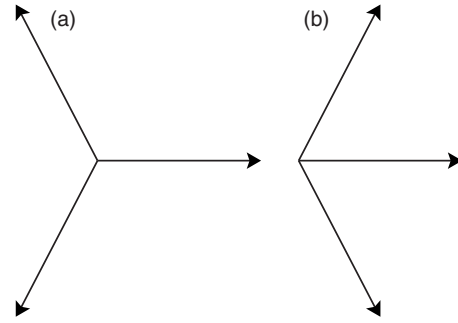


FIG. 6. Schematic representation of the TRSB order parameter in the case of three positive interband couplings (left) and two negative and a positive interband couplings (right). The frustration is resolved in a different but related way.

gap on the second electron band will (almost) entirely depend on the gap on the other *electron* band. Thus the relative phase between the gaps opening on the hole and the electron bands will still be determined by the three-band calculation. These (somewhat naive) arguments allow us the hope that our model, despite its simplicity and numerous assumptions, is relevant for the iron pnictides.

One condition of particular relevance to the pnictides is the condition for existence of superconductivity itself—in the two-band model it is $G_2^{12} > U$, ($G_2^{11} = G_2^{22} \equiv U$ is the intraband pairing). For the real three-band order parameter in the limit $\lambda \gg \eta$ this condition becomes $G_2^\lambda > U/\sqrt{2}$, i.e., it is somewhat relaxed.

VI. JOSEPHSON-COUPLED TWO-GAP s' STATE AND SINGLE-GAP s STATE

We can use the model and the results derived so far to study a different problem—a two-gap s' state coupled via Josephson junction to an ordinary s -wave superconductor. This is a situation of real experimental relevance, in light of the recent experiments demonstrating Josephson effect between Pb and an iron-pnictide superconductor;³² a theoretical background is explored in Refs. 33–35. The tunneling of Cooper pairs in this case would like to align the phases of the two (distinct) superconductors—we can model this by introducing negative coupling constant $\lambda \rightarrow -\lambda$ (and $|\lambda| \ll \eta$ —weak coupling). It does not take one much time to realize that the equations for this model can be made identical to the ones for the previous model by a single sign flip in the three-gap order parameters. For example, the real solution $\tilde{\Delta}_2$ now becomes,

$$\{-\theta, 1, 1\}\Lambda \rightarrow \{\theta, 1, 1\}\Lambda. \quad (24)$$

After this change the phase diagram is identical to that on Fig. 5. The model is still frustrated but the frustration is resolved in a different manner—the nontrivial phase angle now brings the η -coupled gaps closer (instead of further away) to the third gap. This is easy to see at the completely degenerate point $\lambda = \eta$ (Fig. 6),

$$\tilde{\Delta}_3^{symm} \rightarrow \{1, e^{i\pi/3}, e^{-i\pi/3}\}\Omega. \quad (25)$$

The model with negative Josephson junctions still does not

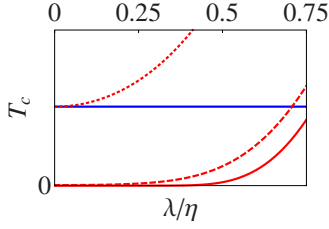


FIG. 7. (Color online) Comparison of the T_c for $\tilde{\Delta}_1$ (blue) and $\tilde{\Delta}_2$ (red) for $b=0$ (solid line), $b=0.5$ (dashed line), and $b=1$ (dotted line). η is fixed. For small λ the two-gap solution is the first to appear for $b < 1$. At the crossing point there is degeneracy and complex $\tilde{\Delta}$ is possible.

give us two *independent* superconductors. To achieve this we add intraband attraction on the weakly coupled band. Now even at $\lambda=0$ we have two different superconducting states—a single-gap s -wave and s' -wave two-gap solutions (previously λ solely was driving the superconductivity on the third band). The equation for T_c becomes,

$$I \begin{pmatrix} -b\eta & -\lambda & -\lambda \\ -\lambda & 0 & \eta \\ -\lambda & \eta & 0 \end{pmatrix} \begin{pmatrix} \Delta^1 \\ \Delta^2 \\ \Delta^3 \end{pmatrix} = - \begin{pmatrix} \Delta^1 \\ \Delta^2 \\ \Delta^3 \end{pmatrix}, \quad (26)$$

where we have parameterized the intraband attraction as a fraction b of η . For the experimental setup of a conventional low-temperature superconductor coupled to iron pnictide sample we expect $b < 1$. The eigenvalues and eigenvectors now are,

$$\delta_i = -I\eta, \quad \frac{I}{2} [\eta(1-b) \mp \sqrt{8\lambda^2 + \eta^2(1+b)^2}], \quad (27)$$

$$\tilde{\Delta}_i \propto \begin{pmatrix} 0 \\ -1 \\ 1 \end{pmatrix}, \quad \begin{pmatrix} \frac{\eta(1+b) \pm \sqrt{8\lambda^2 + \eta^2(1+b)^2}}{2\lambda} \\ 1 \\ 1 \end{pmatrix}. \quad (28)$$

Again there are two possible order parameters. The T_{ci} curves (Fig. 7) still cross but their crossing point is no longer at $\lambda = \eta$. It moves to the left, which is easy to understand—the T_c line for the three-gap OP goes to a finite limit rather than zero for $\lambda \rightarrow 0$ (single-gap SC, courtesy of the nonzero b).

We again expand the gap equations in the vicinity of T_c up to second order in the magnitudes of the superconducting gaps. The two-gap solution is unchanged and the real three-gap solution equations become,

$$\left[(\lambda\theta - \eta) - (\lambda\theta^3 - \eta) \frac{2\lambda + b\eta\theta}{2\lambda + b\eta\theta^3} \right] \ln \left(\frac{2\omega_c}{\pi T} \right) - (\eta - \lambda\theta^3) \frac{\theta}{2\lambda + b\eta\theta^3} - 1 = 0,$$

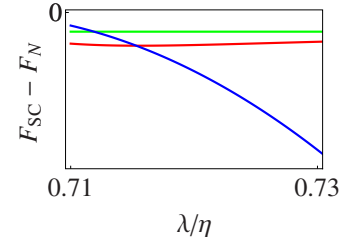


FIG. 8. (Color online) Comparison between the $\mathcal{F}_{SC} - \mathcal{F}_N$ for $\tilde{\Delta}_1$ (green), $\tilde{\Delta}_2$ (blue), and $\tilde{\Delta}_3$ (red) for $b=0.5$. We show calculation for $T=0.95T_c$ at the vicinity of the T_{ci} crossing point $\lambda \approx 0.71\eta$. The interval for which the complex OP minimizes the free energy is smaller but still exists.

$$\theta = \gamma(2\lambda + b\eta\theta) \ln \left(\frac{2\omega_c}{\pi T} \right) - (2\lambda + b\eta\theta^3) \beta_0 \frac{\Lambda^2}{T_c^2}. \quad (29)$$

The complex order-parameter equations are,

$$\lambda\kappa(1 - \kappa^2) \ln \left(\frac{2\omega_c}{\pi T} \right) + \frac{\lambda\kappa^3}{\eta} - \frac{\eta\lambda\kappa}{(b\eta^2 + \lambda^2)} = 0, \quad (30)$$

$$\cos \varphi = \frac{\eta\lambda\kappa}{2(b\eta^2 + \lambda^2)}, \quad \frac{1}{\eta} = \gamma \ln \left(\frac{2\omega_c}{\pi T} \right) - \beta_0 \frac{\Omega^2}{T_c^2}.$$

For $b \rightarrow 0$ these equations reduce correctly to the interband-couplings-only case. We derive single-variable Ginzburg-Landau free energy and then minimize it with respect to Λ and Ω . The comparison between the different solutions for $b=0.5$ is shown in Fig. 8. The result is very similar to the $b=0$ case but the region in which the complex order parameter dominates is smaller. The reason is that the real three-gap solution's free energy is pushed down by the intraband term. However, for $b \rightarrow 1$ the region again expands as the crossing point is pushed closer to $\lambda=0$. For $b > 1$ the real three-gap solution minimizes the \mathcal{F} for all λ , at least for $T \approx T_c$.

Now we discuss the $T=0$ line of the phase diagram. The gap equations for $\tilde{\Delta}_2$ and $\tilde{\Delta}_3$ are now,

$$\theta_0^2 - \frac{\eta}{\lambda} \theta_0 [1 - b(1 + \eta \ln \theta_0)] - 2\theta_0 \ln \theta_0 - 2 = 0,$$

$$\Lambda_0 = 2\omega_c e^{-\theta_0(1+b\eta \ln \theta_0)/(2\lambda+b\eta\theta_0)}$$

and

$$\lambda\kappa_0 \ln(\kappa_0) - \kappa_0 \left(\frac{\lambda^2 - \eta^2}{\lambda\eta} \right) - b \frac{\eta}{\lambda} \kappa_0 (1 - \eta \ln \kappa_0) = 0,$$

$$\cos \varphi_0 = \frac{\eta\kappa_0}{2\lambda} (1 - b + b\eta \ln \kappa_0), \quad \Omega_0 = 2\omega_c e^{-1/\eta}.$$

We compare the energies for the different possible ground states on Fig. 9. Consistent with the results from the T_c region, the complex solution is still the ground state on the left of some λ_{cr} . However, because the energy of $\tilde{\Delta}_2$ is pulled down for nonzero b , the transition a weakly first-order one and λ_{cr} is on the left of the T_{ci} crossing point.

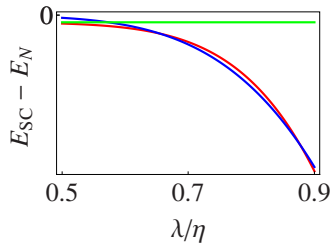


FIG. 9. (Color online) Comparison between the $\mathcal{E}_{\text{SC}} - \mathcal{E}_N$ for the different order parameters. Here $b=0.5$. The energies for $\tilde{\Delta}_2$ and $\tilde{\Delta}_3$ cross for $\lambda_{cr} \approx 0.65$.

With increase in b , λ_{cr} moves to the left, but there is always a region (confined to lower and lower temperatures and smaller and smaller λ as b goes up) in which the complex solution is the preferred order parameter.

VII. CONCLUSIONS

In summary, we have considered a simple microscopic model, with three bands coupled via repulsive pair-scattering interactions, which is relevant for the recently discovered iron-based family of high-temperature superconductors. We have constructed the phase diagram of this model and discussed its overall features. Generally, we find three possible superconducting order parameters, one of which breaks the time-reversal symmetry in order to relax some of the frustration intrinsic to the three (or odd) band case. The conditions for such exotic state are rather strict and it seems unlikely

that this order parameter would be observed in the optimally doped iron pnictides. However, this state may be realistically present in overdoped samples, if the doping is carefully tuned to the range of optimized frustration. While quantitative aspects of our results are bound to be sensitive to the details of the band structure and the accompanying orbital character of each individual iron-pnictide material—the details which are not part of our model—the overall qualitative features reported in this paper are expected to remain relatively universal. Experimental observation of a time-reversal symmetry-breaking superconducting state is perhaps the best we can hope for in linking an s' superconductor to some broken symmetry and would represent arguably the strongest confirmation yet of the basic picture which places the repulsive, purely electron-electron interband interactions at the heart of iron-based high-temperature superconductivity. Furthermore, we have also considered the case of Josephson-coupled two-band s' SC and a single-gap s SC. Again, there is possible time-reversal symmetry-breaking state, although frustration in that case is relieved in a different (but related) manner.

ACKNOWLEDGMENTS

We are grateful to V. Cvetković for useful discussions. Work at the Johns Hopkins-Princeton Institute for Quantum Matter was supported by the U. S. Department of Energy, Office of Basic Energy Sciences, Division of Materials Sciences and Engineering, under Award No. DE-FG02-08ER46544.

-
- ¹Y. Kamihara, T. Watanabe, M. Hirano, and H. Hosono, *J. Am. Chem. Soc.* **130**, 3296 (2008).
- ²X. H. Chen, T. Wu, G. Wu, R. H. Liu, H. Chen, and D. F. Fang, *Nature (London)* **453**, 761 (2008).
- ³G. F. Chen, Z. Li, D. Wu, G. Li, W. Z. Hu, J. Dong, P. Zheng, J. L. Luo, and N. L. Wang, *Phys. Rev. Lett.* **100**, 247002 (2008).
- ⁴Z. A. Ren, G. C. Che, X. L. Dong, J. Yang, W. Lu, W. Yi, X. L. Shen, Z. C. Li, L. L. Sun, F. Zhou, and Z. X. Zhao, *EPL* **83**, 17002 (2008).
- ⁵H. H. Wen, G. Mu, L. Fang, H. Yang, and X. Zhu, *EPL* **82**, 17009 (2008).
- ⁶M. Rotter, M. Tegel, and D. Johrendt, *Phys. Rev. Lett.* **101**, 107006 (2008).
- ⁷G. F. Chen, Z. Li, G. Li, W. Z. Hu, J. Dong, X. D. Zhang, P. Zheng, N. L. Wang, and J. L. Luo, *Chin. Phys. Lett.* **25**, 3403 (2008).
- ⁸A. J. Drew, Ch. Niedermayer, P. J. Baker, F. L. Pratt, S. J. Blundell, T. Lancaster, R. H. Liu, G. Wu, X. H. Chen, I. Watanabe, V. K. Malik, A. Dubroka, M. Roessle, K. W. Kim, C. Baines, and C. Bernhard, *Nat. Mater.* **8**, 310 (2009).
- ⁹H. Chen, Y. Ren, Y. Qui, W. Bao, R. H. Liu, G. Wu, T. Wu, Y. L. Xie, X. F. Lang, Q. Huang, and X. H. Chen, *EPL* **85**, 17006 (2009).
- ¹⁰I. I. Mazin, D. J. Singh, M. D. Johannes, and M. H. Du, *Phys. Rev. Lett.* **101**, 057003 (2008).
- ¹¹K. Kuroki, S. Onari, R. Arita, H. Usui, Y. Tanaka, H. Kontani, and H. Aoki, *Phys. Rev. Lett.* **101**, 087004 (2008).
- ¹²V. Cvetković and Z. Tešanović, *EPL* **85**, 37002 (2009).
- ¹³S. Graser, T. A. Maier, P. J. Hirschfeld, and D. J. Scalapino, *New J. Phys.* **11**, 025016 (2009).
- ¹⁴A. V. Chubukov, D. V. Efremov, and I. Eremin, *Phys. Rev. B* **78**, 134512 (2008).
- ¹⁵F. Wang, H. Zhai, Y. Ran, A. Vishwanath, and D.-H. Lee, *Phys. Rev. Lett.* **102**, 047005 (2009).
- ¹⁶V. Cvetković and Z. Tešanović, *Phys. Rev. B* **80**, 024512 (2009).
- ¹⁷M. M. Parish, J. Hu, and B. A. Bernevig, *Phys. Rev. B* **78**, 144514 (2008); K. Seo, B. A. Bernevig, and J. Hu, *Phys. Rev. Lett.* **101**, 206404 (2008).
- ¹⁸P. Goswami, P. Nikolic, and Q. Si, [arXiv:0905.2634](https://arxiv.org/abs/0905.2634) (unpublished), and references therein.
- ¹⁹H. Suhl, B. T. Matthias, and L. R. Walker, *Phys. Rev. Lett.* **3**, 552 (1959).
- ²⁰V. A. Moskalenko, *Fiz. Met. Metalloved.* **8**, 503 (1959) [*Phys. Met. Metallogr.* **8**, 25 (1959)].
- ²¹J. Kondo, *Prog. Theor. Phys.* **29**, 1 (1963).
- ²²K. Nakayama, T. Sato, P. Richard, Y.-M. Xu, Y. Sekiba, S. Souma, G. F. Chen, J. L. Luo, N. L. Wang, H. Ding, and T. Takahashi, *EPL* **85**, 67002 (2009).
- ²³For studies of a two-band model in the context of iron pnictides see, for example, V. Stanev, J. Kang, and Z. Tesanovic, *Phys.*

- Rev. B **78**, 184509 (2008); V. Barzykin and L. P. Gor'kov, *JETP Lett.* **88**, 131 (2008); L. Benfatto, M. Capone, S. Caprara, C. Castellani, and C. Di Castro, *Phys. Rev. B* **78**, 140502(R) (2008); and O. V. Dolgov, I. I. Mazin, D. Parker, and A. A. Golubov, *ibid.* **79**, 060502(R) (2009). A more realistic four-band model was studied by L. Benfatto, E. Cappelluti, and C. Castellani, *ibid.* **80**, 214522 (2009) but the frustration effects were not considered there.
- ²⁴I. Eremin and A. Chubukov, *Phys. Rev. B* **81**, 024511 (2010).
- ²⁵T. K. Ng and N. Nagaosa, *EPL* **87**, 17003 (2009).
- ²⁶W.-C. Lee, S.-C. Zhang, and C. Wu, *Phys. Rev. Lett.* **102**, 217002 (2009).
- ²⁷D. F. Agterberg, V. Barzykin, and L. P. Gor'kov, *Phys. Rev. B* **60**, 14868 (1999).
- ²⁸For a brief introduction to the properties of superconductors with broken time-reversal symmetry see M. Sigrist, *Physica B* **280**, 154 (2000), and references therein.
- ²⁹A. V. Chubukov, M. G. Vavilov, and A. B. Vorontsov, *Phys. Rev. B* **80**, 140515(R) (2009).
- ³⁰R. Thomale, C. Platt, J. Hu, C. Honerkamp, and B. A. Bernevig, *Phys. Rev. B* **80**, 180505(R) (2009).
- ³¹Y. Ren, J. H. Xu, and C. S. Ting, *Phys. Rev. B* **53**, 2249 (1996).
- ³²X. Zhang Y. S. Oh, Y. Liu, L. Yan, K. H. Kim, R. L. Greene, and I. Takeuchi, *Phys. Rev. Lett.* **102**, 147002 (2009).
- ³³I. B. Sperstad, J. Linder, and A. Sudbø, *Phys. Rev. B* **80**, 144507 (2009).
- ³⁴P. Ghaemi, F. Wang, and A. Vishwanath, *Phys. Rev. Lett.* **102**, 157002 (2009).
- ³⁵M. Araujo and P. Sacramento, *J. Phys.: Conf. Ser.* **200**, 012008 (2010).